

Dynamics of monolayer xenon adsorbed on Pt(111)

R. D. Boutchko* and L. W. Bruch

Department of Physics, University of Wisconsin-Madison, Madison, Wisconsin 53706, USA

(Received 24 May 2004; revised manuscript received 3 September 2004; published 16 November 2004)

Effects of substrate dynamics for xenon adsorbed on the (111) face of platinum are calculated using realistic xenon interatomic potentials, force constants for the platinum that reproduce the bulk lattice dynamics, and the Barker-Rettner semiempirical Xe-Pt potential. There is only a minor change in the platinum density of states when the coupling of harmonic normal modes of the xenon monolayer solid to the platinum substrate is included. Effects of the dynamic coupling on the xenon are small, apart from the previously known Brillouin-zone-center mixing, both for the simply commensurate $\sqrt{3}R30^\circ$ lattice and for a possible denser $\sqrt{19}$ -commensurate unit cell with seven Xe atoms. The frequency spectra are calculated for four other hypothetical higher-order commensurate xenon lattices with average lattice spacings close to those for experimentally observed triangular incommensurate Xe/Pt(111) lattices, but assuming a static substrate. Compared to the $\sqrt{3}$ Xe lattice, the spectrum $\omega_\perp(q)$ of perpendicular Xe vibrations of the other lattices is shifted to lower frequencies and is greatly broadened. This significant calculated dispersion of $\omega_\perp(q)$ is counter to experiment for incommensurate monolayer xenon. Also, the coefficient of Brownian friction for a single Xe adatom on Pt(111) is evaluated.

DOI: 10.1103/PhysRevB.70.195422

PACS number(s): 68.43.-h

I. INTRODUCTION

A xenon monolayer adsorbed on the close-packed face of platinum, Xe/Pt(111), incorporates elements of physical adsorption and of chemical adsorption and a wide range of phenomena are manifest. Its structure is varied continuously^{1,2} by adjusting the thermo-mechanical forces, a characteristic of physisorption, but the energetics and optimal atomic adsorption site are more characteristic of chemisorption.³ It has been studied with a great variety of experimental techniques and there are rather successful *a priori* calculations of the Xe-Pt(111) interaction potential.^{4,5} So much is known and understood that any remaining contradictions between experimental data and the results of statistical mechanical modeling take on increased significance. The purpose of this paper is to examine the effect on the modeling of including the dynamical coupling of the monolayer to the substrate and to treat more complex monolayer structures than were included in previous calculations.

The Xe/Pt(111) monolayer was the subject of pioneering experiments on sublimation of the monolayer solid,⁶ the hybridization of monolayer and substrate vibrations,⁷ the phonon dispersion relations of the monolayer solid,⁸ the dynamics of the monolayer gas,⁹ and imaging the relief of the incommensurate solid.^{10,11} A proposal¹² that the optimal adsorption site of a single xenon atom is on top of a platinum surface atom led to much further work on the generality of the effect.¹³⁻¹⁵

A semiempirical potential¹⁶ for the interaction of Xe with Pt(111), constructed by Barker and Rettner to fit many properties including sticking coefficients, was successful in describing some later data.¹⁷ However, quasielastic helium scattering experiments⁹ from a 2D gas of Xe/Pt(111) are interpreted as showing the surface is less corrugated than that of the Barker-Rettner potential. Also, although the measured frequencies^{7,8,17} ω_\perp of perpendicular xenon vibrations are

very similar for the 2D gas, the commensurate solid and the incommensurate solid, calculations¹⁸ for the commensurate solid and for a solid floating on the laterally averaged potential indicated there should have been observable differences. These considerations suggest that the surface is less corrugated than that of the Barker-Rettner potential, but recent calculations^{4,5} for Xe/Pt(111) yield surfaces with more energy corrugation. Two major concerns remaining from previous theoretical work are as follows: (1) What is the ground-state monolayer lattice on this surface? Scanning tunneling microscope images¹⁰ of the monolayer solid show there are incommensurate submonolayer islands at low temperature. (2) What effect does the corrugation have on the frequency spectrum of the triangular incommensurate lattices of Xe/Pt(111)? Might there be a subtle cancellation and net reduction of the corrugation effects in a more detailed calculation than that¹⁸ done previously? This paper mainly addresses the second concern and shows that the large effects for the Barker-Rettner surface persist in the more detailed analysis.

The organization of this paper is as follows: Section II contains the definition of the monolayer lattices and a summary of the components of the interaction model and the methods of evaluating the lattice dynamics. Section III presents results for the Brownian friction of a xenon atom on Pt(111) and for the coupled lattice dynamics of the observed $\sqrt{3}$ and possible $\sqrt{19}$ commensurate Xe/Pt lattices. Section IV presents results for the dispersion of phonon frequencies of hypothetical higher-order-commensurate monolayers of Xe on a static Pt(111) substrate. Concluding remarks are given in Sec. V.

II. METHODS**A. Structures**

The substrate is the (111) surface of platinum, an fcc solid. With a nearest-neighbor spacing $\ell = 2.77 \text{ \AA}$, primitive vectors of the surface are

TABLE I. Possible higher-order commensurate lattices of Xe/Pt(111) generated by the Bravais lattice defined in Eq. (4). There are $3M^2+3M+1$ surface Pt atoms in the unit cell and N^2 Xe atoms. L is the nearest-neighbor spacing of the average Xe lattice and ϑ the rotation angle of the Bravais lattice relative to the $[11\bar{2}]$ (30°) azimuth of the Pt surface. [Except for the $\sqrt{19}$ case, the ϑ 's are within 0.2° of the angles calculated for triangular incommensurate lattices of Xe/Pt(111) with the same L using the perturbation theory of Novaco and McTague. See Ref. 8.]

M	N	L (Å) ^a	Misfit m	ϑ	Experiment ^b
4	5	4.327	0.0982	3.67°	$\sim 3.3^\circ$
5	6	4.404	0.0821	3.00°	$\sim 2.5^\circ$
6	7	4.459	0.0705	2.54°	$\sim 0^\circ$
7	8	4.501	0.0618	2.20°	
" $\sqrt{19}$ "		4.564	0.0487	4.31°	

$$^a L = (1/N) \sqrt{(3M^2 + 3M + 1)\ell} \equiv L_{\sqrt{3}}(1 - m).$$

^b Interpolated in Kern's data (Ref. 33).

^c Parameters for the HOC lattice defined at Eq. (3). The ϑ is that for the leading reciprocal vector of the average xenon lattice relative to the $[11\bar{2}]$ Pt azimuth; see Refs. 19 and 36.

$$\mathbf{a}_1 = \ell \hat{x}, \quad \mathbf{a}_2 = \ell \left(\frac{1}{2} \hat{x} + \frac{\sqrt{3}}{2} \hat{y} \right). \quad (1)$$

Then the primitive vectors of the $(\sqrt{3} \times \sqrt{3})R30^\circ$ lattice of xenon atoms on Pt(111) are

$$\mathbf{A}_1(\sqrt{3}) = \mathbf{a}_1 + \mathbf{a}_2, \quad \mathbf{A}_2(\sqrt{3}) = 2\mathbf{a}_2 - \mathbf{a}_1, \quad (2)$$

of length $\sqrt{3}\ell = 4.80$ Å. The xenon atoms are situated on top of Pt surface atoms at a distance of about¹⁵ 3.4 Å.

A possible higher-order commensurate lattice with only a few xenon atoms in the unit cell and nearest-neighbor spacing in the range observed for monolayer xenon solids is generated^{19,20} by putting seven Xe atoms in a unit cell with primitive vectors

$$\mathbf{A}_1(\sqrt{19}) = 3\mathbf{a}_1 + 2\mathbf{a}_2, \quad \mathbf{A}_2(\sqrt{19}) = -2\mathbf{a}_1 + 5\mathbf{a}_2 \quad (3)$$

of length $\sqrt{19}\ell$ and the average Xe-Xe spacing is $L = \sqrt{19}/7\ell \approx 4.56$ Å. However, this structure has not been observed for Xe/Pt(111).

Another family²¹ of possible higher-order commensurate (HOC) lattices is formed from primitive vectors

$$\mathbf{A}_1 = (M+1)\mathbf{a}_1 + M\mathbf{a}_2, \quad \mathbf{A}_2 = -M\mathbf{a}_1 + (2M+1)\mathbf{a}_2, \quad (4)$$

with the Bravais cell containing N^2 Xe atoms at positions generated initially by the vectors $\mathbf{b}_1 = \mathbf{A}_1/N$; $\mathbf{b}_2 = \mathbf{A}_2/N$. The four sets of M, N in Table I cover much of the density range of observed triangular incommensurate lattices of Xe/Pt(111) and are used here to model substrate lattice effects on the rotated hexagonally incommensurate phase of Xe/Pt(111).

In these calculations, the Pt atoms are assumed to form a perfect fcc lattice with no relaxation of the surface layers. For the $(\sqrt{3} \times \sqrt{3})R30^\circ$ commensurate Xe/Pt(111) lattice, the overlayer spacing $z \approx 3.33$ Å is that which minimizes the

static potential energy. For the higher-order commensurate lattices, the positions of the Xe atoms are adjusted by simulated annealing or force relaxation to give configurations of minimum static potential energy. The lattice dynamics are evaluated for the relaxed structures, i.e., for Bravais cells which are not uniformly compressed.

B. Interactions and lattice dynamics

The basic interaction model consists of the HFD-B2 Xe-Xe pair potential,²² the 4NN set of force constants of Bortolani *et al.*²³ to reproduce the bulk platinum lattice dynamics, and the Barker-Rettner¹⁶ Xe-Pt potential. It is supplemented by the McLachlan substrate-mediated dispersion force,²⁴ which has been found^{16,25,26} to improve the description of the Xe/Pt(111) monolayer phase diagram.

The dynamics are treated in the harmonic approximation,²⁷ and the calculations are straightforward in principle. The dynamical coupling of the monolayer and substrate is evaluated using the explicit dependence of the Barker-Rettner potential¹⁶ on the positions of both Xe and Pt atoms. In the implementation for the dynamically coupled system, the substrate is modeled using finite-thickness slabs.²⁸ It is now routine to treat wave vectors throughout the surface Brillouin zone for simply commensurate monolayers. However, for the first four HOC lattices of Table I, the substrate is taken to be static and the dynamic adlayer-substrate coupling is neglected.

Surface properties of the platinum substrate, such as the Brownian friction,²⁹ were evaluated with slabs of up to 120 layers of platinum atoms. The coupled $(\sqrt{3} \times \sqrt{3})R30^\circ$ commensurate Xe/Pt(111) monolayer solid was treated with a 75 layer platinum slab. For the higher-order commensurate lattice with 7 Xe atoms in a triangular cell with 19 Pt surface atoms, Sec. III C, only 15 layers were used for the platinum slab. These slabs sufficed for convergence of the calculated properties reported here.

The data resulting from the lattice dynamics calculations for the j normal mode branches are the frequencies $\omega_j(\mathbf{q})$ and eigenvectors $\mathbf{e}^j(\mathbf{q})$. These are presented as a set of dispersion curves for specified 2D wave vector \mathbf{q} and as density of states functions $\rho_\perp(\omega)$ and $\rho_\parallel(\omega)$ in which the frequencies are weighted with the perpendicular and parallel components, respectively, of the Xe or surface Pt atoms, ($\alpha = \perp, \parallel$).

$$\rho_\alpha(\Omega) = \sum_j \frac{1}{A_{Br}} \int |\mathbf{e}_\alpha^j(\mathbf{q})|^2 \delta(\omega_j(\mathbf{q}) - \Omega) d^2q. \quad (5)$$

In Eq. (5), the integral is done over the area A_{Br} of the 2D Brillouin zone, and the subscript α on the eigenvector picks out the atoms and Cartesian components for the appropriate density of states. The functions ρ_α are evaluated using Brillouin zone sampling methods.^{30,31} The $\rho_\alpha(\Omega)$ for the coupled monolayer-substrate calculations are constructed using histograms with frequency bin-width 0.035 THz ≈ 0.15 meV.

III. COUPLED XENON AND PLATINUM DYNAMICS

A. Brownian friction

The Brownian friction is evaluated²⁹ using the two leading corrugation amplitudes V_g (i.e., $g = g_0 = 4\pi/\ell\sqrt{3}$ and g

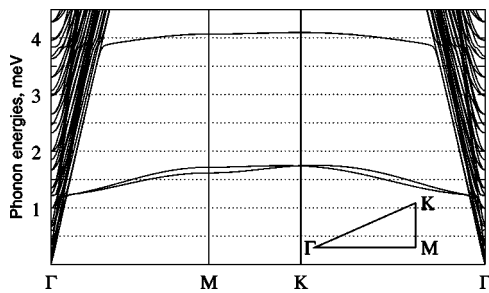


FIG. 1. Phonon dispersion curves of the $\sqrt{3}R30^\circ$ Xe/Pt(111) coupled commensurate monolayer as a function of wave number along the Γ - M - K - Γ monolayer azimuths. The lowest three branches are the parallel and perpendicular Xe modes. Platinum modes extend to 29 meV (1 THz=4.13 meV), but this presentation is truncated at 4.5 meV to enable a better display of the Xe modes. The inset shows the irreducible sector of the Brillouin zone; the wave numbers at the M and K points are 0.756 and 0.873 \AA^{-1} , respectively.

$=g_0\sqrt{3}$) of the Barker-Rettner Xe-Pt potential and the lattice dynamics of thick Pt slabs. Average values over a surface unit cell are $\gamma([1\bar{1}0])=1.2 \times 10^8 \text{ sec}^{-1}$ and $\gamma([11\bar{2}])=1.8 \times 10^8 \text{ sec}^{-1}$, along two noted azimuths of Pt(111). Both are consistent with an upper limit of 0.25 ps^{-1} on the friction coefficient set by Ellis *et al.*⁹ from analysis of the quasielastic helium scattering experiments on a low density 2D Xe gas. As in the Brownian friction calculations²⁹ for Kr and N_2 on graphite, there is a large variation (factor of 100 between maximum and minimum) with lateral position in the unit cell. The reported averages are formed using values at the height of minimum potential energy at many points in the surface unit cell. Tests were made for numerical convergence with respect to sampling of the wave vectors in the surface Brillouin zone and to the slab thickness. A slab with 100 layers sufficed to determine the γ s to 25%.

B. Coupling of modes for the $\sqrt{3}$ commensurate layer

The dispersion curves in Fig. 1 show the normal modes of the xenon monolayer and the hybridization with substrate modes at small $|q|$. The results are quite similar to those obtained⁷ with an elasticity theory for the substrate response. The hybridization and damping of adlayer vibrational modes when they overlap a continuum of substrate modes have been demonstrated experimentally for several adatom-substrate combinations and are rather well understood.^{7,32}

Figure 2 shows the frequency density of states of surface Pt atoms. For modes polarized parallel to the surface plane, there is no noticeable difference between the results for bare Pt(111) and with this commensurate Xe monolayer. On the scale of the histogram bin widths ($\approx 0.15 \text{ meV}$), there are barely discernible differences in the density of states of the perpendicular modes for the coupled/uncoupled calculations in the range 8–16 meV. The reaction of the platinum substrate to the xenon monolayer is much smaller than that found in the corresponding calculations for the $\sqrt{3}$ lattice of krypton on graphite.³⁰ This may be explained by the weak coupling between graphite planes making the perpendicular

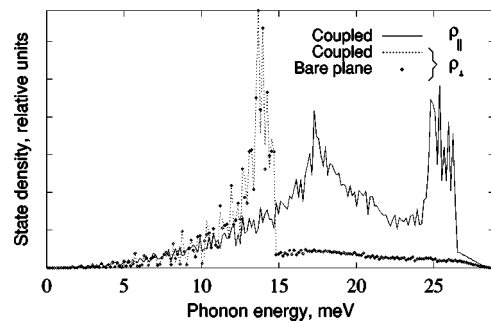


FIG. 2. Density of states of surface Pt atom vibrations as a function of energy for motions parallel (ρ_{\parallel}) and perpendicular (ρ_{\perp}) to the Pt(111) plane. Results are shown for the bare Pt surface and for the coupled $\sqrt{3}R30^\circ$ Xe/Pt(111). There are no noticeable differences for modes polarized in the surface plane and only a slight difference for the perpendicular modes at 8–16 meV, with shifts of spectral features scarcely larger than the 0.15 meV bin-width of the histogram.

modes of carbon atoms more susceptible to influence by the adsorbate.

Figures 3(a) and 3(b) show the density of states of xenon modes polarized parallel and perpendicular to the monolayer plane. There are broadenings of the zone-center gap frequencies $\omega_{0\parallel}$ and $\omega_{0\perp}$ by mixing with the platinum modes. The mixing introduces lower frequency components for the in-plane density of states (compare the frequencies outside the mixing region in Fig. 1). For the out-of-plane motions there is a mixing of higher frequency components, as noted in previous experimental work.^{7,8} Experimentally, at 80 K the S-mode has¹⁷ $\omega_{\perp}=3.5 \text{ meV}$, with small dispersion. These calculations are at 0 K and it is known¹⁸ that thermal expansion perpendicular to the plane reduces $\omega_{0\perp}$ by about 0.4 meV , so that there is a good level of agreement between the calculations and experiments.

C. Coupling of modes for the $\sqrt{19}$ higher-order commensurate lattice

Besides the $\sqrt{3}$ commensurate lattice, uniaxially incommensurate and triangular incommensurate monolayer solids are observed for Xe/Pt(111). One question that arises is

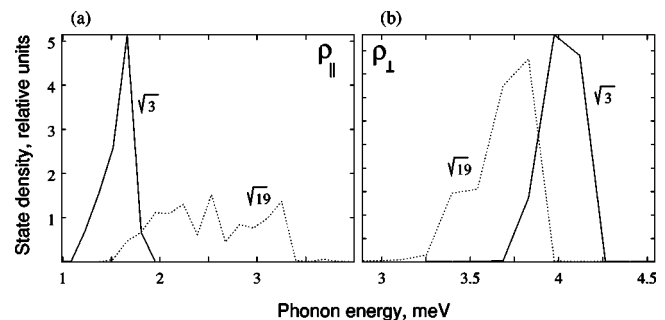


FIG. 3. Density of states of Xe atom modes as a function of energy for the $\sqrt{3}$ and $\sqrt{19}$ commensurate monolayers coupled to Pt(111), with the B2M interaction model. Vibrations (a) parallel and (b) perpendicular to the Pt(111) plane.

TABLE II. Properties of several possible monolayer lattices of Xe/Pt(111) in the static substrate approximation. Lengths are in Å and energies in meV. The unit cells of the lattices are given by Eqs. (2)–(4). L is the nearest-neighbor spacing of the average Xe lattice. V is the total potential energy per Xe atom and E the ground state energy per atom including the zero-point energy of the phonons. The height differences Δz (in Å) are $z_{max} - z_{min}$ for the Xe atoms in the corresponding minimum potential energy configuration. The calculations are for the Barker-Rettner surface (Ref. 16). Two Xe-Xe pair potentials are used: the HFD-B2 model (Ref. 22) (“B2”) and that model augmented by the McLachlan interaction (Ref. 24) (“B2M”). The Xe-Xe interactions are truncated at 12.3 Å and the Xe/Pt(111) corrugation series is truncated at the fourth shell of reciprocal lattice vectors. Calculations used Pt lattice constant $\ell = 2.77$ Å.

L	“ M, N ”	$V(\text{B2})$	Δz^d	$E(\text{B2})$	$V(\text{B2M})$	Δz^d	$E(\text{B2M})$
4.33	4,5 ^a	-316.48	0.215	-311.79	-303.73	0.282	-299.14
4.40	5,6 ^a	-316.85	0.213	-312.49	-304.91	0.272	-300.65
4.46	6,7 ^a	-316.61	0.246	-312.42	-305.17	0.301	-301.09
4.50	7,8 ^a	-316.28	0.204	-312.20	-305.24	0.265	-301.24
4.56 ^b	$\sqrt{19}$	-310.34	0.178	-306.92	-300.30	0.219	-296.92
4.80 ^c	$\sqrt{3}$	-314.28	0	-310.90	-305.82	0	-302.43

^aLattices specified by Eq. (4); see Table I.

^bLattice specified by Eq. (3).

^c($\sqrt{3} \times \sqrt{3}$) R30° lattice, Eq. (2).

^dThe difference in heights of minimum potential energy at the 3-fold fcc site and the atop site is 0.242 Å on the Barker-Rettner surface, 0.09 Å on the Betancourt-Bird surface (Ref. 5) and 0.12 Å on the Da Silva *et al.* surface (Ref. 4). Estimates for the variation in height for incommensurate monolayers derived from STM experiments (Ref. 10) are $\bar{L} = 4.37 \pm 0.05$ Å and $\Delta z \approx 0.17$ Å; $\bar{L} = 4.43 \pm 0.05$ Å and $\Delta z \approx 0.14$ Å.

whether there is any noticeable change in the reaction of the substrate for structural changes in the monolayer. Another is what changes in the spectrum of the Xe $\omega_{\perp}(q)$ branch, relative to Figs. 1 and 3 for the $\sqrt{3}$ commensurate lattice, arise because the adatoms are not all in the same substrate environment.

To address these questions with unit cells of moderate size we considered two hypothetical higher-order commensurate lattices. One with 4 Xe atoms in a triangular cell of 13 Pt surface atoms could be treated in great detail³⁰ but had the disadvantage that the average Xe-Xe spacing of 5.00 Å led to many unstable Xe vibrational modes polarized in the surface plane. The second is the $\sqrt{19}$ lattice defined in Eq. (3) with an average Xe-Xe spacing 4.56 Å, closer to those observed for Xe monolayers. It does not have dynamical instabilities. With 15 Pt layers, repetitious calculations of phonon dispersion relations remain quite feasible. Thus this is a good case in which to test for coupling effects. The fact that only very small effects on modes polarized parallel to the surface plane are found gives new support to the use of a static substrate approximation for higher-order commensurate lattices with more atoms in the unit cell.

The densities of states for Xe motions parallel and perpendicular to the surface plane are shown in Fig. 3. The $\omega_{\perp}(q)$ now has a great dispersion, with some spectral density in the range 0.8–2.9 meV and a reduction of the spectral density near 3.5 meV. There is still some spectral density above 3.7 meV, consistent with the mixing of higher frequencies near the zone center discussed for the $\sqrt{3}$ lattice in Sec. III B. The overall trends for $\omega_{\perp}(q)$ are understood in terms of the z modulation of the monolayer solid, in which the heights of the seven-atom unit cell range from 3.35 to 3.48 Å. For the $\sqrt{3}$ lattice the heights were 3.33 Å.

For a Xe solid at height 3.44 Å on the laterally averaged Barker-Rettner surface the frequency would be¹⁸ $\omega_{\perp} = 2.6$ meV.

IV. PHONONS OF HIGHER-ORDER COMMENSURATE LATTICES

The observed³³ triangular incommensurate lattices of Xe/Pt(111) have average nearest-neighbor spacings L of 4.33 to 4.49 Å and orientational epitaxy rotation angles (relative to $[11\bar{2}]$ Pt azimuth) that decrease from 3.3° to 1° as L increases from 4.33 to 4.45 Å. The phonon spectrum of the $L \approx 4.33$ Å lattice was measured^{7,8} by inelastic helium atom scattering. Its S-mode has nearly no dispersion, $\omega_{\perp} = 3.40 \pm 0.05$ meV, but there is spectral density at about 3.8 meV when the mode overlaps bulk Pt phonon bands. We infer from the calculations reported in Secs. III B and III C that the monolayer phonons may be evaluated accurately with a static substrate model, except near the Brillouin zone center, and therefore do such calculations for all the higher-order commensurate lattices defined in Table I. We also compare the total potential energy V and total energy E including zero-point energy as part of the study on what the ground state structure is.³⁴

The energies V and E , per atom, are presented in Table II for all the lattices treated in this paper. The results illustrate how sensitively the decision on the ground state structure depends on the interaction model. For the model B2M including the McLachlan interaction, generally^{16,25,26} thought to be a necessary part of the interaction, the $\sqrt{3}$ lattice is the most stable of those listed. For the model B2 with only the “bare” pair potential HFD-B2 based on 3D data, the most stable of the lattices is for $L \approx 4.40$ Å. The inference from

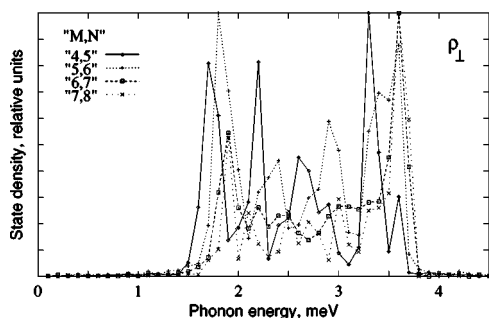


FIG. 4. Density of states ρ_{\perp} as a function of energy for Xe vibrations perpendicular to the Pt(111) plane for four hypothetical higher order commensurate lattices listed in Table I. The ρ_{\perp} are scaled to have the same total normalization.

the experiments^{2,10,35} is that the most stable lattice at low temperatures (no entropy effects, minimum energy, sub-monolayer islands) is a triangular incommensurate lattice with $L \approx 4.45$ Å. For a revised model to reproduce this conclusion will require a tradeoff of adjustments to the corrugation of the Xe/Pt(111) potential and to the adsorption-induced Xe-Xe interactions.

In spite of the “stiffening” of frequencies of in-plane modes for the $\sqrt{3}$ lattice by the formation of the Brillouin-zone-center frequency gap, the average zero-point energy for that lattice is the smallest of any of the structures in Table II except in one case, the $E(B2M)$ for the $\sqrt{19}$ lattice. The effect of the zone-center gap generally is outweighed in the total zero-point energy by the decrease of frequencies ω_{\parallel} at other parts of the zone and the average ω_{\perp} is reduced in the higher-order commensurate lattices relative to that for the $\sqrt{3}$ lattice.

Figure 4 shows the spectral densities $\rho_{\perp}(\omega)$ of the perpendicular (z) motion calculated for the four higher-order commensurate monolayer lattices constructed using Eq. (4). These data, for a static substrate, supplement the results for the $\sqrt{19}$ lattice on a dynamic substrate shown in Fig. 3.

The Barker-Rettner surface is so corrugated that the calculated $\omega_{\perp}(q)$ has much more dispersion than is observed. There is no significant dispersion of $\omega_{\perp}(q)$ in experiments^{1,7,8,17} for Xe/Pt(111). The calculations also differ from observations and calculations for incommensurate monolayers of argon and krypton on graphite.³⁷ The calculated dispersion for Xe/Pt(111) arises from an unusual z -dependence of the leading corrugation amplitude V_{g0} of the Barker-Rettner potential. In the Steele decomposition³ of the Xe-Pt potential using reciprocal lattice vectors of the Pt(111) surface,

$$V_h(\vec{r}, z) = V_0(z) + \sum_{\vec{g}} V_{\vec{g}}(z) \exp(i\vec{g} \cdot \vec{r}), \quad (6)$$

the leading contribution to ω_{\perp} is from d^2V_0/dz^2 . For the heights z of the modulated monolayers, the contribution decreases with increasing height, $d^3V_0/dz^3 < 0$. At these distances the energy amplitude V_{g0} calculated for the Barker-Rettner potential has $V_{g0} < 0$ and $dV_{g0}/dz > 0$. However $d^2V_{g0}/dz^2 > 0$ and the corrugation adds to the force constant for ω_{\perp} in the $\sqrt{3}R30^\circ$ commensurate lattice. In the incommensurate layers, the average height z is larger and the coherent contribution of the corrugation is smaller. That is, these effects add for the Barker-Rettner potential and lead to the substantial change in ω_{\perp} obtained in the calculations. For other systems,³⁷ the corresponding effects are offsetting and the net dispersion in ω_{\perp} is small.

V. CONCLUSIONS

The calculations for the coupled dynamics for two examples of commensurate xenon monolayer and platinum substrate show that (i) there is scarcely any reaction of the platinum atoms to the adsorbate and (ii) the principal effect of the substrate dynamics is in hybridization near the Brillouin zone center. An evaluation of the coefficient of Brownian friction is consistent with an upper bound placed by quasielastic helium atom scattering for a dilute 2D gas of Xe on Pt(111) and, also, supports analysis of the Xe atom mobility with neglect of substrate dynamics.

These calculations have identified an unusual feature of the energy corrugation in the very successful Barker-Rettner potential energy surface for Xe/Pt(111). That feature is directly responsible for a calculated dispersion in ω_{\perp} that is in contradiction to experimental data. Two other indications of problems with the potential energy surface are the amount of height variation in incommensurate monolayers inferred from STM measurements and the fact that the ground state monolayer lattice at temperatures below 30 K is a triangular incommensurate lattice. The progress^{4,5} with *a priori* calculations may help with the revisions that are needed to construct the next generation model.

ACKNOWLEDGMENTS

This work has been partially supported by NSF-DMR9807410 and DMR0104300. We thank Professor A. D. Novaco for a summary of his calculations.

*Present address: Dept. of Medical Physics, University of Wisconsin-Madison, Madison WI 53706.

¹G. Comsa, K. Kern, and B. Poelsema, in *Helium Atom Scattering from Surfaces*, edited by E. Hulpke (Springer, Berlin, 1992), pp. 243–263; K. Kern and G. Comsa, in *Phase Transitions in Surface Films 2*, edited by H. Taub *et al.* (Plenum, New York,

1991), pp. 41–65; P. Zeppenfeld, U. Becher, K. Kern, and G. Comsa, *J. Electron Spectrosc. Relat. Phenom.* **54**, 265 (1990).

²K. Kern, R. David, P. Zeppenfeld, and G. Comsa, *Surf. Sci.* **195**, 353 (1988).

³L. W. Bruch, M. W. Cole, and E. Zaremba, *Physical Adsorption: Forces and Phenomena* (Oxford, New York, 1997).

- ⁴J. L. F. Da Silva, C. Stampfl, and M. Scheffler, *Phys. Rev. Lett.* **90**, 066104 (2003).
- ⁵A. E. Betancourt and D. M. Bird, *J. Phys.: Condens. Matter* **12**, 7077 (2000).
- ⁶B. Poelsema, L. K. Verheij, and G. Comsa, *Phys. Rev. Lett.* **51**, 2410 (1983).
- ⁷B. Hall, D. L. Mills, P. Zeppenfeld, K. Kern, U. Becher, and G. Comsa, *Phys. Rev. B* **40**, 6326 (1989), and references therein.
- ⁸L. W. Bruch, A. P. Graham, and J. P. Toennies, *J. Chem. Phys.* **112**, 3314 (2000).
- ⁹J. Ellis, A. P. Graham, and J. P. Toennies, *Phys. Rev. Lett.* **82**, 5072 (1999).
- ¹⁰F. Brunet, R. Schaub, S. Féderigo, R. Monot, J. Buttet, and W. Harbich, *Surf. Sci.* **512**, 201 (2002).
- ¹¹P. S. Weiss and D. M. Eigler, *Phys. Rev. Lett.* **69**, 2240 (1992).
- ¹²J. M. Gottlieb, *Phys. Rev. B* **42**, 5377 (1990); J. E. Müller, *Phys. Rev. Lett.* **65**, 3021 (1990).
- ¹³J. Henk and R. Feder, *J. Phys.: Condens. Matter* **6**, 1913 (1994); P. Zeppenfeld, G. Comsa, and J. Barker, *Phys. Rev. B* **46**, 8806 (1992).
- ¹⁴M. Potthoff, G. Hilgers, N. Müller, U. Heinzmann, L. Haunert, J. Braun, and G. Borstel, *Surf. Sci.* **322**, 193 (1995).
- ¹⁵Th. Seyller, M. Caragiu, R. D. Diehl, P. Kaukasoina, and M. Lindroos, *Phys. Rev. B* **60**, 11 084 (1999); R. D. Diehl, Th. Seyller, M. Caragiu, G. S. Leatherman, N. Ferralis, K. Pussi, P. Kaukasoina, and M. Lindroos, *J. Phys.: Condens. Matter* **16**, S2839 (2004).
- ¹⁶J. A. Barker and C. T. Rettner, *J. Chem. Phys.* **97**, 5844 (1992); **101**, 9202(E) (1994).
- ¹⁷L. W. Bruch, A. P. Graham, and J. P. Toennies, *Mol. Phys.* **95**, 579 (1998). Correction to the caption of Fig. 1a: the beam energy was 22.18 meV.
- ¹⁸L. W. Bruch and A. D. Novaco, *Phys. Rev. B* **61**, 5786 (2000).
- ¹⁹The starting point is a uniform triangular lattice with Xe atoms in the $\sqrt{19}$ Bravais cell at positions $\mathbf{b}_1=(\mathbf{A}_1+2\mathbf{A}_2)/7$; $\mathbf{b}_2=2\mathbf{b}_1$; $\mathbf{b}_3=3\mathbf{b}_1$; $\mathbf{b}_4=\mathbf{b}_1+(3\mathbf{A}_1-\mathbf{A}_2)/7$; $\mathbf{b}_5=\mathbf{b}_4+\mathbf{b}_1$; $\mathbf{b}_6=\mathbf{b}_5+\mathbf{b}_1$; $\mathbf{b}_7=0$, using the primitive vectors defined in Eq. (3). The primitive vector \mathbf{b}_1 of the average lattice is rotated from the Pt lattice vector \mathbf{a}_2 by 4.3° .
- ²⁰The stability of this structure for Xe/Pd(111) is in dispute. Its occurrence there has been attributed to effects of contamination. See J. F. Zhu, H. Ellmer, H. Malissa, T. Brandstetter, D. Semred, and P. Zeppenfeld, *Phys. Rev. B* **68**, 045406 (2003), and references therein.
- ²¹K. Kern, R. David, R. L. Palmer, and G. Comsa, *Appl. Phys. A: Solids Surf.* **A41**, 91 (1986).
- ²²A. K. Dham, W. J. Meath, A. R. Allnatt, R. A. Aziz, and M. J. Slaman, *Chem. Phys.* **142**, 173 (1990).
- ²³V. Bortolani, A. Franchini, G. Santoro, J. P. Toennies, Ch. Wöll, and G. Zhang, *Phys. Rev. B* **40**, 3524 (1989); see also R. F. Wallis, A. A. Maradudin, V. Bortolani, A. G. Eguiluz, A. A. Quong, A. Franchini, and G. Santoro, *ibid.* **48**, 6043 (1993).
- ²⁴A. D. McLachlan, *Mol. Phys.* **7**, 381 (1964). The coefficients for Xe/Pt are $C_{s1}=201$ a.u. and $C_{s2}=154$ a.u. The effective overlayer spacing relative to the imaging surface plane is calculated from the distance z to the surface layer of Pt atoms by $L_{ov}=z-(d/2)$ where the interplanar spacing of the Pt lattice is $d=\sqrt{2/3}\ell=2.26$ Å.
- ²⁵P. A. Rejto and H. C. Andersen, *J. Chem. Phys.* **98**, 7636 (1993).
- ²⁶J. M. Gottlieb and L. W. Bruch, *Phys. Rev. B* **44**, 5759 (1991).
- ²⁷M. Born and K. Huang, *Dynamical Theory of Crystal Lattices* (Oxford, New York, 1954) (reprinted 1988).
- ²⁸E. de Rouffignac, G. P. Alldredge, and F. W. de Wette, *Phys. Rev. B* **24**, 6050 (1981), and references therein.
- ²⁹R. D. Boutchko and L. W. Bruch, *Phys. Rev. B* **59**, 10 992 (1999). Corrected values for the average Brownian coefficients reported there are: Kr/graphite $\gamma_x=0.63$; $\gamma_y=0.85$ and $\text{N}_2/\text{graphite}$ $\gamma_x=3.1$; $\gamma_y=4.2$; all in units of 10^9 sec^{-1} .
- ³⁰R. D. Boutchko, Ph.D. thesis, University of Wisconsin–Madison, 2001. The calculations were performed with $\ell=2.774$ Å, the value of the lattice constant at 25°C .
- ³¹S. L. Cunningham, *Phys. Rev. B* **10**, 4988 (1974); D. J. Chadi and M. L. Cohen, *ibid.* **8**, 5747 (1973).
- ³²L. W. Bruch and F. Y. Hansen, *Phys. Rev. B* **55**, 1782 (1997), and references therein.
- ³³K. Kern, *Phys. Rev. B* **35**, 8265 (1987).
- ³⁴A. D. Novaco, in unpublished zero-temperature calculations with the same interaction model using SCP and QHT dynamics (defined in Ref. 18), found the $\sqrt{3}$ -lattice to be unstable to an incommensurate state, probably uniaxially incommensurate rather than rotated triangular incommensurate or higher-order triangular commensurate phases.
- ³⁵K. Kern, R. David, R. L. Palmer, and G. Comsa, *Phys. Rev. Lett.* **56**, 620 (1986).
- ³⁶In more detail, the leading reciprocal lattice vectors \vec{t}_i of the average lattice are given in terms of those ($\vec{\tau}_j$) of the HOC cell defined with $\vec{A}(\sqrt{19})$ by $\vec{t}_1=\vec{\tau}_1+3\vec{\tau}_2$ and $\vec{t}_2=2\vec{\tau}_1-\vec{\tau}_2$. Even after relaxation of the seven atomic positions in the unit cell, the most intense static structure factors are \vec{t}_1 and \vec{t}_2 .
- ³⁷L. W. Bruch, *Phys. Rev. B* **68**, 235420 (2003), and references therein.